Collisional EPR Frequency Shifts in Cs-Rb-Xe Mixtures

S. Zou†, D.J. Morin, C. Weaver, Z. Armanfard, J. Muschell, A.I. Nahlawi, and B. Saam*

Department of Physics & Astronomy, Washington State University, P.O. Box 642814, Pullman, WA 99164-2814, USA

I. The Enhancement Factor κ_0

- Characterizes alkali-metal wave function overlap with noble-gas nucleus
- Relevant to understanding SEOP [1] physics
- Important for understanding systematic shifts occurring in magnetometers
- Precise value can be used to calibrate noble-gas polarimetry

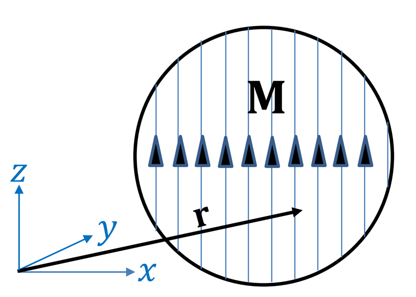

MAGNETIZED SPHERE

Through-space contribution to the total B-field is zero **everywhere** inside uniformly magnetized sphere; only contribution at any interior point $\mathbf{r}$ is $(8\pi/3)\delta(\mathbf{r})\mathbf{M}$. κ_0 characterizes the *amplification* of the noble-gas magnetization to the alkali-metal effective field relative to the classical magnetostatic case.

EPR FREQUENCY SHIFT [2]

$$\Delta|f_A| = \left|\frac{df_A}{dB_0}\right| \underbrace{\frac{8\pi}{3}\mu_X \frac{\langle K_z\rangle}{K}[X]\kappa_0}_{\text{Field}}$$

Noble-gas magnetization M_X

EFFECTIVE GYROMAGNETIC RATIO

$$\left.\left|\frac{df_A}{dB_0}\right|\right|_{I\pm1/2} = \frac{1}{h}\frac{|g_s|\mu_B}{2I+1}\left(1 \mp \frac{2\overline{m}_F|g_s|\mu_B}{A(2I+1)}B_0 + \mathcal{O}(B_0{}^2)+\cdots\right)$$

Low-field limit for alkali-metal atom gyromagnetic ratio.

Quadratic Zeeman term

II. Rb-Cs "Hybrid" Cells

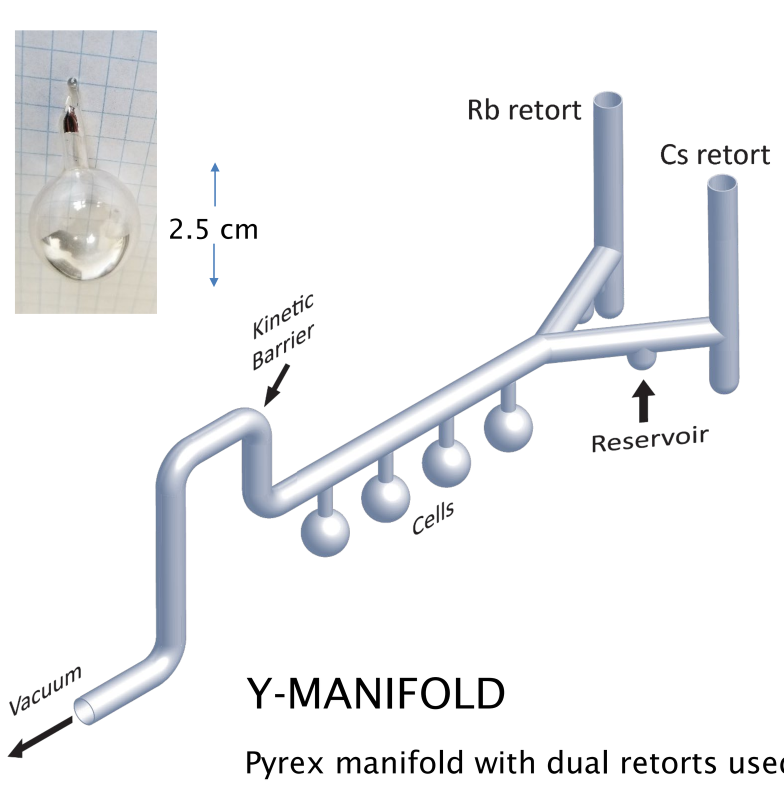

Y-MANIFOLD

Pyrex manifold with dual retorts used to distill in Cs and Rb metals separately into each cell.

CELL	V_{Rb}/V_{Cs}	^{4}He	N_2	Xe
304A	8.3 ± 2.9	1912 ± 52	57.7 ± 1.6	40.1 ± 1.3
304B	8.3 ± 2.9	1932 ± 53	57.0 ± 1.6	40.4 ± 1.4
304C	10.0 ± 3.7	1951 ± 53	56.6 ± 1.5	32.5 ± 1.4

- V_{Rb}/V_{Cs} is volume ratio of macroscopic (solid/liquid) alkali-metals Rb and Cs in the cell
- Pressures in torr at 20 ºC
- Xe enriched to 90% ^{129}Xe.

III. The Embedded Alkali-Metal Magnetometer

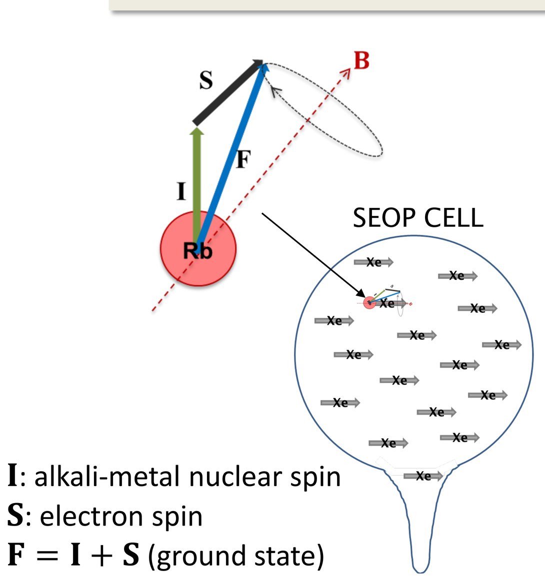

I: alkali-metal nuclear spin
S: electron spin
F = **I** + **S** (ground state)

We use nearest-neighbor hyperfine transitions to detect the alkali-metal EPR frequency shift due to the magnetic field produced by noble-gas atoms as they are polarized (by SEOP) and depolarized (by NMR pulses) in a vapor cell.

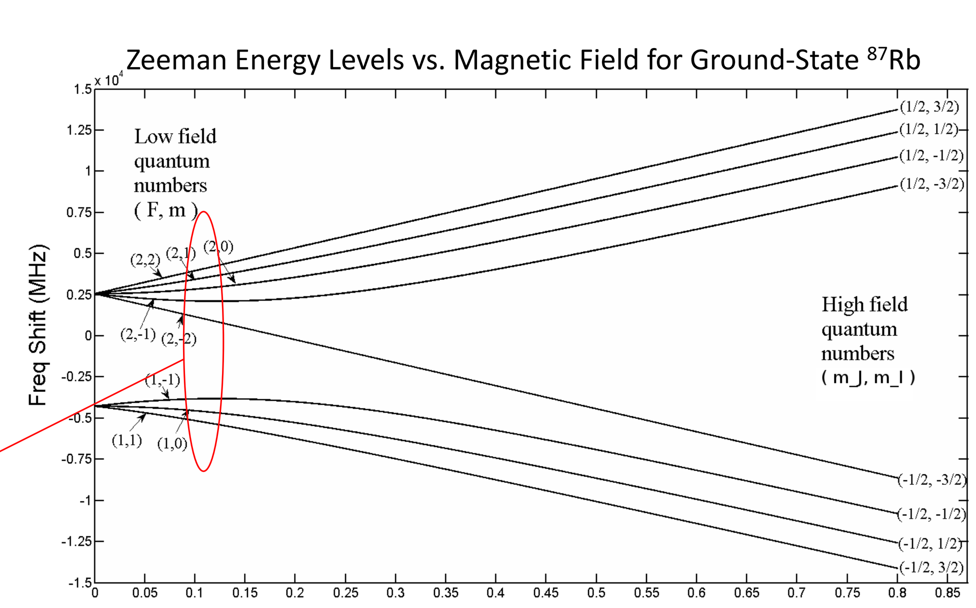

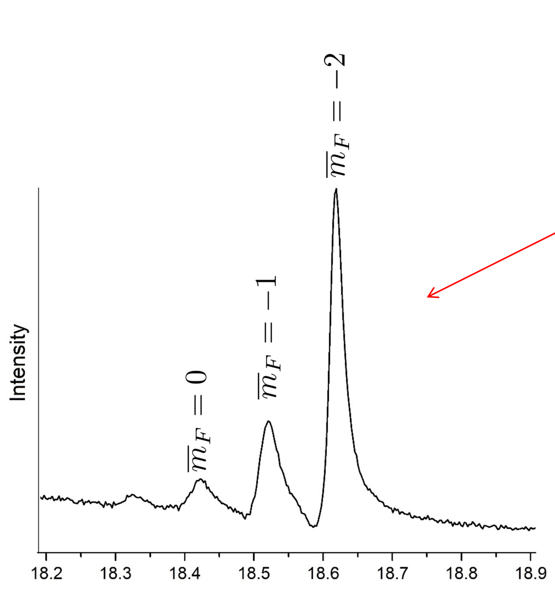

OPTICAL PUMPING WITH NUCLEAR SPIN

Optical pumping drives ground-state population toward one of the two end states in the $F = I + 1/2$ hyperfine manifold having maximum $|m_F|$.

IV. Optically Detected EPR

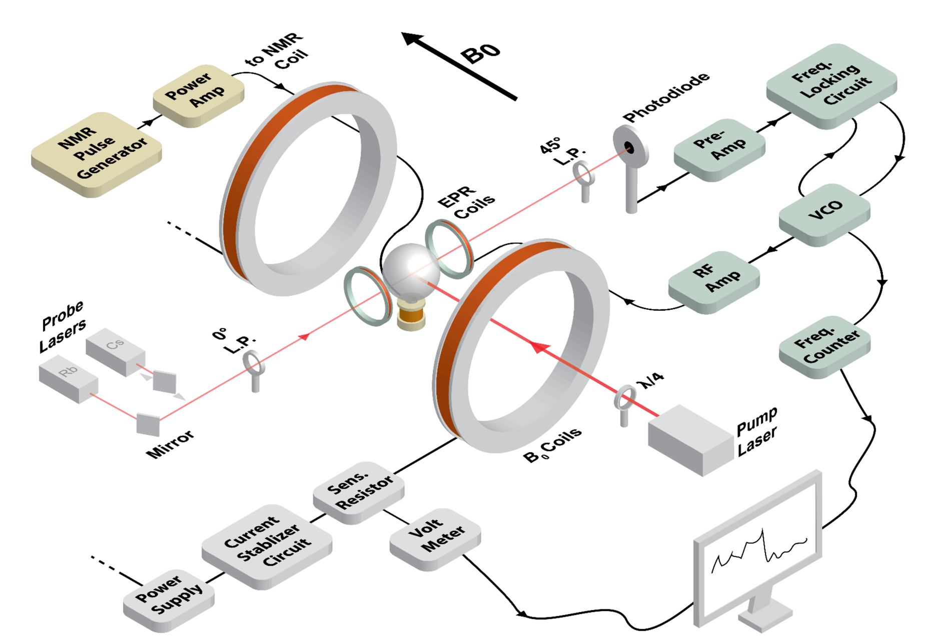

Experimental apparatus: more detail, particularly for locking circuitry, is in Ref. [3]. Dual probe lasers (one each for Rb and Cs EPR) with a pick-off mirror are positioned to swap rapidly between Rb and Cs EPR

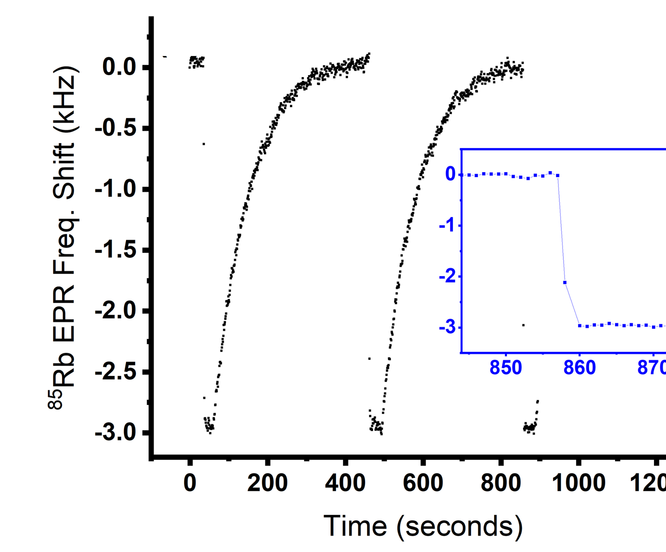

Representative data for ^{85}Rb. The EPR frequency is locked to the sensed magnetic field. The sharp drops indicate when ^{129}Xe nuclear polarization was suddenly destroyed by a comb of resonant NMR pulses.

V. The Light-Shift Systematic

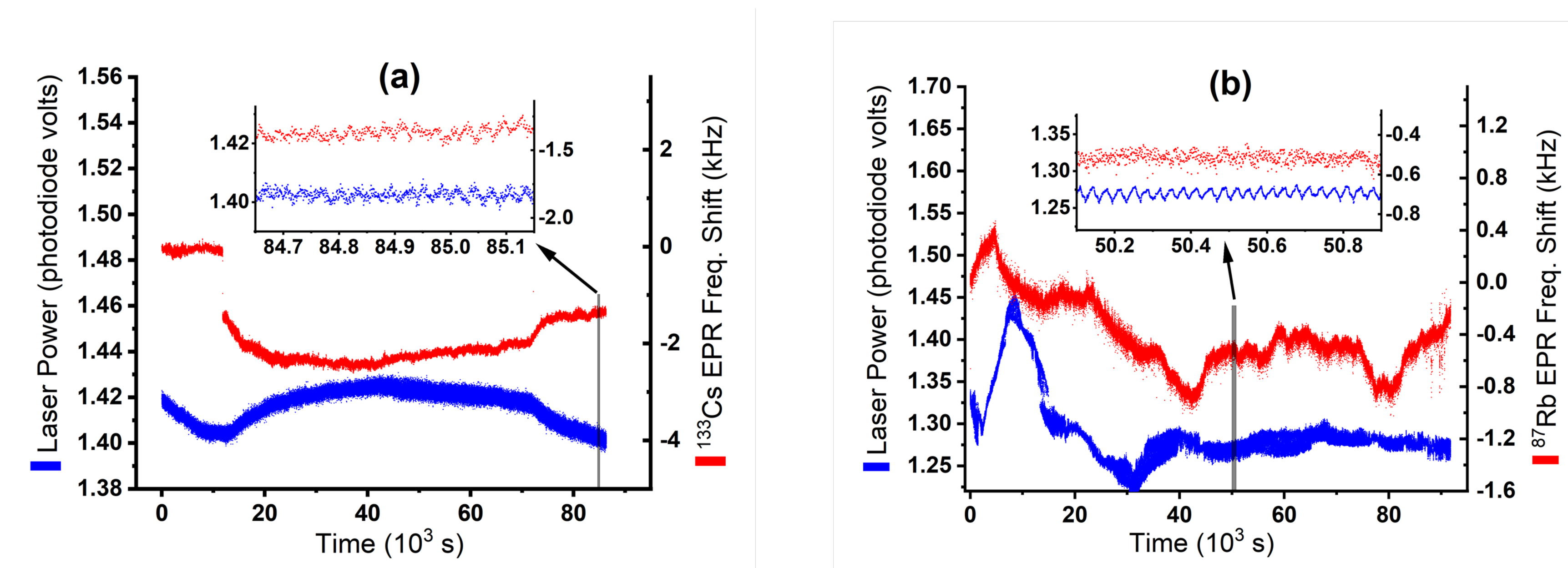

(a) Plot of ^{133}Cs EPR frequency shift overlayed with plot of relative Cs-D_1 pump-laser power vs. time. The cell contains no Xe or other polarizable noble-gas species. Variations in the pump laser power produce correlated light-shift variations in the locked EPR frequency on both long and short (inset) time scales. Nominal pump-laser power was 28.5 W. (b) Same as (a) except that the ^{87}Rb EPR frequency shift is overlayed with the Cs-D_1 pump-laser power. Since probed atom and pumped atom are different, no correlation is observed on any time scale. The EPR-shift fluctuations are also much smaller overall in (b), where light-shift effects are absent.

VI. EPR Shift Ratio $\Delta f(^{85}Rb)/\Delta f(^{133}Cs)$

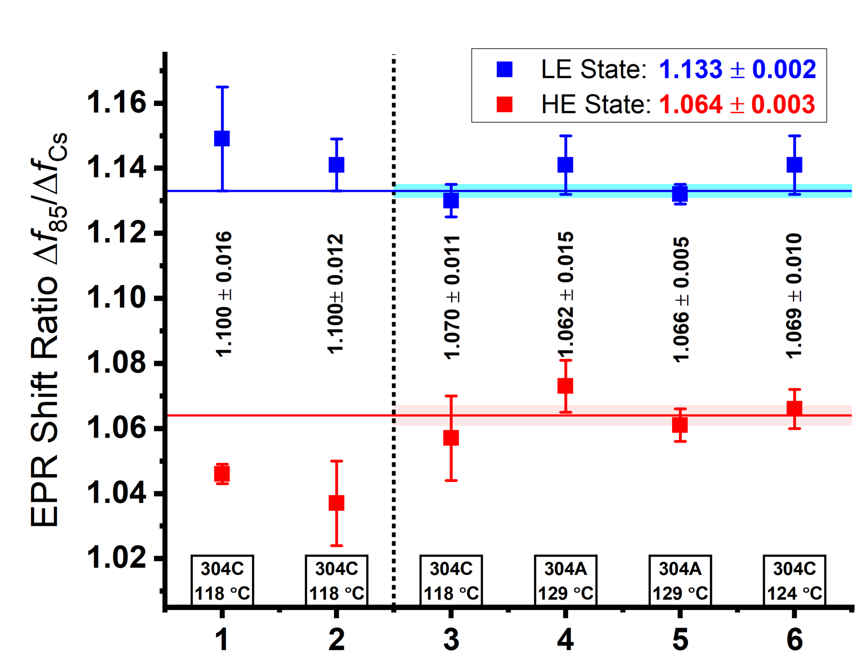

Ratio of successive EPR frequency shifts (^{85}Rb vs. ^{133}Cs) resulting from the sudden destruction of the same ^{129}Xe magnetization in hybrid (Rb/Cs) vapor cells. High-energy (HE) and low-energy (LE) optical pumping Zeeman states ($\overline{m}_F = \pm I$) yield different values because they have different effective gyromagnetic ratios (Section I). Data to the left of the dashed line were acquired before we understood light-shift noise from the pump laser; only data to the right of the line are included in the analysis. The "ratio of ratios" (blue point divided by red point) for each trial is a systematic check on the result, since the ratio depends only on the precisely known effective gyromagnetic ratios. For trials 3-6, this ratio is within 1% of the expected value.

VII. Final Results, κ_0 for CsXe

$$\frac{(\kappa_0)_{\text{CsXe}}}{(\kappa_0)_{\text{RbXe}}} = \frac{\Delta f_{\text{Cs}}}{\Delta f_{\text{Rb}}}\left(\frac{\gamma'_{\text{Rb}}}{\gamma'_{\text{Cs}}}\right) = 1.215 \pm 0.007$$

Using: $(\kappa_0)_{\text{RbXe}} = 518 \pm 8$ (Our earlier work [3]):

$$(\kappa_0)_{\text{CsXe}} = 629 \pm 10$$

- Both $(\kappa_0)_{\text{RbXe}}$ and $(\kappa_0)_{\text{CsXe}}$ are 25% below theoretical prediction of Walker [4], but the ratio of the two agrees well with [4].
- Our result for $(\kappa_0)_{\text{CsXe}}$ is more precise, but not inconsistent with previous measurement by Jian-Chen, et al. [5]:

$(\kappa_0)_{\text{CsXe}} = 702 \pm 41$ @ 80 °C $(\kappa_0)_{\text{CsXe}} = 653 \pm 20$ @ 90 °C

- Our results show no temperature dependence over the 115-135 ºC range studied.

REFERENCES/FOOTNOTES

†Present address: Beihang University, 37 Xueyuan Road, Haidian District, Beijing, 100191, China

*brian.saam@wsu.edu

[1]T.G. Walker and W. Happer, *Rev. Mod. Phys.* **69**, 629 (1997).
[2] S.R. Schaefer, *et al.*, *Phys. Rev. A* **39**, 5613 (1989).
[3] A.I. Nahlawi, et al., *Phys. Rev. A* **100**, 053415 (2019).
[4] T.G. Walker, *Phys. Rev. A* **40**, 4959 (1989).
[5] F. Jian-Cheng, *et al.*, *Chin. Phys. B* **23**, 063401 (2014).

ACKNOWLEDGEMENTS

We are grateful to glassblower Aaron Babino at Clear Horizons Laboratory Glass Services for vapor cell and manifold fabrication. We acknowledge support for this work from the U.S. National Science Foundation, grant PHY-0953225 and our GOALI partner, Polarean, Inc.

NSF PHY-0953225

POLAREAN BREATHTAKING IMAGES